J Mater Sci: Mater Electron (2017) 28:295–303
DOI 10.1007/s10854-016-5524-z

Crystal structure and magnetism of $BiFeO_3$ nanoparticles regulated by rare-earth Tb substitution

QiaoXia Xing[1] · Zhonglin Han[1] · Shifeng Zhao[1]

Received: 18 June 2016 / Accepted: 8 August 2016 / Published online: 12 August 2016

Abstract Tb-doped $BiFeO_3$ nanoparticles were prepared using sol–gel method. The effect of Tb substitution on crystal structure and magnetism of $BiFeO_3$ nanoparticles were investigated. It is shown that the crystal structure and magnetism of $BiFeO_3$ nanoparticles are regulated by rare-earth Tb substitution. Particularly, the sizes of the particles are reduced to smaller than 100 nm after doping with Tb. The magnetization of Tb-doped $BiFeO_3$ nanoparticles has been enhanced in magnitude, which is mainly attributed to the suppression of spin cycloid structure belonging to R3c phase fraction in the process of rhombohedral-to-orthorhombic structural phase transformations. At the meantime, the magnetic hysteresis loops show exchange bias towards negative axis. The exchange bias behaviors originate from the coupling interaction between antiferromagnetic core and ferromagnetic surface. The present work provides a route regulating the magnetization of $BiFeO_3$ particles as well as further promoting its applications in multiferroic materials.

1 Introduction

Multiferroics are defined within this context for materials in which there is a coexistence and coupling of ferroelectric and magnetic ordering parameters [1]. Such magnetoelectrically coupled materials exhibit the ability to switch the magnetic state upon the application of an electric field or vice versa. Multiferroics could create new opportunities for nonvolatile memories with lower power consumption, fast switching speed, and more robust cycling characteristics, as well as other novel spintronic-based applications such as antennae, motors, or sensors [2]. As one of most outstanding multiferroic material, $BiFeO_3$ has attracted enormous curiosities because of its high ferroelectric Curie temperature ($T_C \sim 1103$ K) and G-type antiferromagnetic order below Néel temperature ($T_N \sim 643$ K) [3, 4], which makes it favorable to exhibit magnetoelectric coupling at and above room temperature. Multiferroic $BiFeO_3$ based heterostructures have captured immense interest due to their potential applications in nondestructive and high density integrated memory devices [5, 6]. However, the G-type antiferromagnetic order and this spin structure which modified by a spin cycloid with periodicity of 62 nm along axis cancel the net macroscopic magnetization and inhibit linear magnetoelectric effect [7].

Hence, suppressing the spiral spin structure becomes an important route to enhance the magnetic properties. At present, there are two ways to suppress the spiral spin structure. One is to result in lattice mismatch with larger or smaller cations substitution at A-site or B-site. The rare earth ion substitution at Bi-site has been already established to achieve magnetic enhancement in $BiFeO_3$ via destroying its structure [8]. Another is to make the particle size smaller than 62 nm by increasing dopant concentration and other methods for preparing or applying external force [9–11]. Enhanced magnetism was detected in the BiFeO3 nanorods under room temperature owing to the small diameters [12]. Therefore, size dependent magnetic properties of multiferroic $BiFeO_3$ nanoparticles has been investigated widely and to some degree improved the magnetism [13, 14]. Moreover, uncompensated spins at the

✉ Shifeng Zhao
zhsf@imu.edu.cn

[1] School of Physical Science and Technology, Inner Mongolia Key Lab of Nanoscience and Nanotechnology, Inner Mongolia University, Hohhot 010021, People's Republic of China

surface have been confirmed in this size dependent system through following experiments: one indicated that Fourier Transform Infrared Spectroscopy (FTIR Spectroscopy) peaks of $BiFeO_3$ nanoparticles shift to lower wave number with the decreasing particle size [15], another also shown a shift towards negative axis in the magnetic hysteresis (M–H) loop of $BiFe_{0.95}Sc_{0.05}O_3$ [16]. Though, remarkable achievements have been obtained in both of two systems respectively. Up to now, there is little discussion combined the effect of the crystal structural distortion and the size of nanoparticles on the magnetic properties by regulating rare earth ions substitution. Though rare-earth Tb possesses large magnetic moment, it does not help modulate the magnetic structure of $BiFeO_3$ with its magnetic moment because no long-range magnetic ordering forms in the crystal lattice [17]. And it owns a smaller ionic radius than Bi ion so that Tb ions could enter Bi sites easily. Therefore, it is properly that substituting Bi with Tb to study how the doped cations affect the structure and magnetization magnetism of $BiFeO_3$ particles. $Bi_{1-x}Tb_xFeO_3$ (x = 0, 0.5, 0.1, 0.15 and 0.2) polycrystalline nanoparticles were prepared in this work. The samples have been characterized by several instruments. Following two distinct facts motivate the progress of present work: (a) both lattice constants and interplanar distance reduced with increasing Tb concentration, (b) the magnetic hysteresis (M–H) loops show the exchange bias towards negative axis. The origins of the effect of doping concentration on the structure and magnetism are discussed in detail.

2 Experiment details

The pure and Tb-doped $BiFeO_3$ nanoparticles were prepared using sol–gel method. The precursor materials, including $Bi(NO_3)_3{\cdot}5H_2O$ (3 % excess), $Tb(NO_3)_3{\cdot}6H_2O$ and $Fe(NO_3)_3{\cdot}9H_2O$ with the concentration of 0.025 mol/L in stoichiometric cation ratio were first mixed into dilute nitric acid (HNO_3:H_2O = 4:1). After stirred at 60 °C for 1 h, $C_4H_6O_6$ with the concentration of 0.025 mol/L was also dissolved in above solutions. Then, the solutions were stirred at 60 °C for 3 h unceasingly and dried in hot air oven at 150 °C for about 5 h. Finally, the samples were sintered at 550 °C for 3 h and grinded. X-ray diffraction (XRD, Panalytical Empyrean) measurements were performed with Cu-Kα radiation source to analyze the crystal structure of $Bi_{1-x}Tb_xFeO_3$ particles. The crystal structural phase transformation was analyzed using Rietveld crystal structure refinement software, General Structure Analysis System (GSAS). Further evidence for the quality and composition of the particles was obtained from X-ray photoelectron spectra (XPS) studies. Transmission electron microscopy (TEM) images of the samples were taken through a FEI F20 electron microscope with an accelerating voltage of 200 kV. Physical Property Measurement System (PPMS) was used to measure M–H loops.

3 Results and discussion

Figure 1a shows the XRD patterns of the pure and Tb-doped $BiFeO_3$ particles. The pure $BiFeO_3$ agrees well with the R3c space group of rhombohedral structure as the (104) and (110) diffraction peaks are almost completely separated. With the increasing of Tb-doped concentration x from 0 to 0.20, the positions of all the peaks shift towards higher 2θ values, which originates from a structural distortion of $BiFeO_3$ lattice due to the smaller radius of Tb^{3+} (~0.923 Å) than that of Bi^{3+}(~1.03 Å). Notably, some peaks merge in 10 % Tb-doped $BiFeO_3$ such as: (104) and (110), (006) and (202) etc. And some new diffraction peaks belonging to Pbnm space group appear in $Bi_{1-x}Tb_xFeO_3$ (x = 0.15, 0.2) nanoparticles, for instance: (111), (020), (021) etc. All the phenomena above indicating a new structure like Pbnm has joined in this crystal, which result in lattice distortions. These lattice distortions show a possible influence on the lattice parameter of Tb-substituted $BiFeO_3$ nanoparticles.

Figure 1b further gives an expanded view on the location of diffraction peaks in the range of 20°–35° (2θ). It shows that the peak positions of diffraction peaks shift toward higher diffraction angle 2θ value with the increase of Tb doped concentration, which means that the lattice parameter of $BiFeO_3$ particles is shortened after doping Tb. The corresponding degree of distortion induced by the dopants in perovskite structure was calculated using Goldschmidt tolerance factor [18]:

$$\tau = (<r_A + r_O>)/\sqrt{2}(r_B + r_O) \quad (1)$$

where r_A is the ionic radius of the A-site cations, r_B is that of B-site cations, and r_O is O anions, respectively. In an ideal cubic perovskite without the tilt of oxygen octahedral, the corresponding value of tolerance factor τ exactly equals 1 [19], while the tolerance factor value of $Bi_{1-x}Tb_xFeO_3$ was calculated to be 0.8404, 0.8385, 0.8367, 0.8348 and 0.8330 for x = 0, 0.05, 0.1, 0.15 and 0.2 respectively, which indicates that the distortion increases with the increase of dopants. This kind of distortion arises on account of Tb^{3+} owning smaller radius than that of Bi^{3+}, which leads to the smaller average A-site ionic radius of Tb-doped $BiFeO_3$. This size mismatch between the two A-site cations (Tb^{3+} and Bi^{3+}) gives rise to the chemical stress effect and makes the original R3c structure unstable [20]. Meanwhile, Fe–O and Bi–O bonds are under compression and tension, respectively [21]. In order to

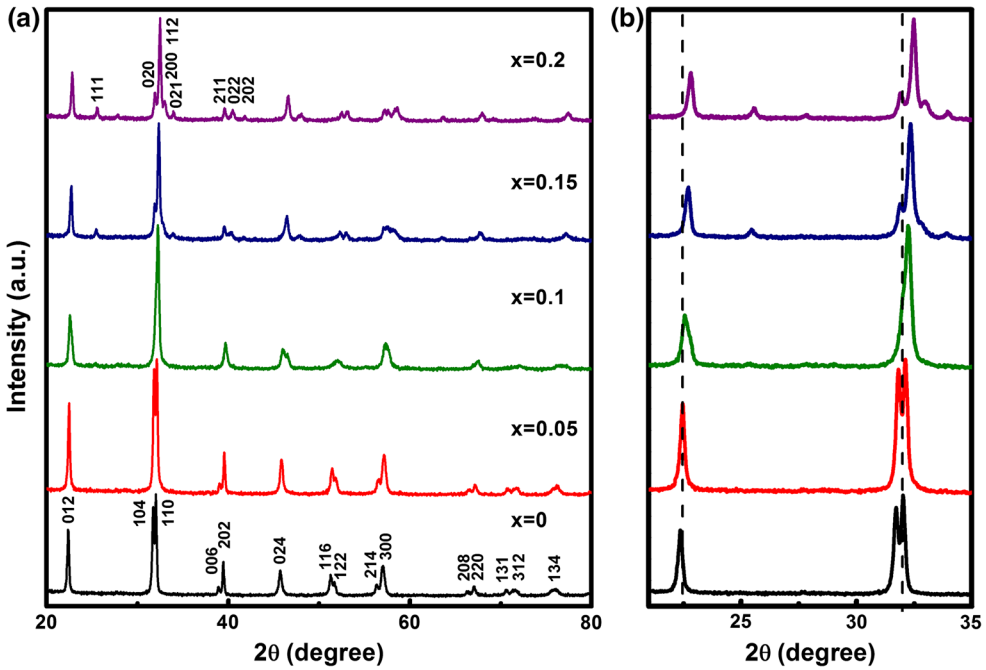

Fig. 1 **a** XRD patterns of the pure and Tb-doped $BiFeO_3$ nanoparticles, **b** an expanded view on the location of diffraction peaks in the range of 20°–35° (2θ)

relieve chemical stress and gain the stabled structural, the lattice parameters (a, c) and unit cell volume (V) belonging to R3c phase decreased. For the sake of confirm this distortion and phase transformation, the XRD patterns were analyzed using the Rietveld refinement method with the GSAS software to calculate the lattice parameters and phase fraction.

Figure 2 exhibits the results of Rietveld refinements. And the optimal goodness of fit [χ^2 (less than 1)] and R-factors [R_p (less than 0.06), R_{wp} (less than 0.09)] as numerical criteria of the fitting quality were obtained. All of the unit cell parameters and reliability factors obtained from the Rietveld refinement analysis are summarized in Table 1. It is shown that pure $BiFeO_3$ are indexed by a rhombohedral structure (R3c), while other samples are indexed by multi-phase states mixed by rhombohedral and orthorhombic (Pbnm) structure. The normalized unit cell parameters including a, c and c/a with the reference of R3c phase show as a function of Tb-doped concentration. From x = 0 to 0.2, the fraction of R3c phase gradually reduces from 1 (x = 0) to 0.7849 (x = 0.05), 0.6695 (x = 0.10), 0.4590 (x = 0.15) to 0.0296 (x = 0.2), respectively. At the same time, the lattice parameters (a, c, V) belonging to R3c phase in the coexistent structural state clearly present a gradual reduction. These changes of unit cell parameters belonging to R3c phase put down to the lattice distortion occurring in the structural transformation from R3c to Pbnm space group due to the smaller ionic radius of Tb^{3+} than that of Bi^{3+}. When Tb doping concentration reaches

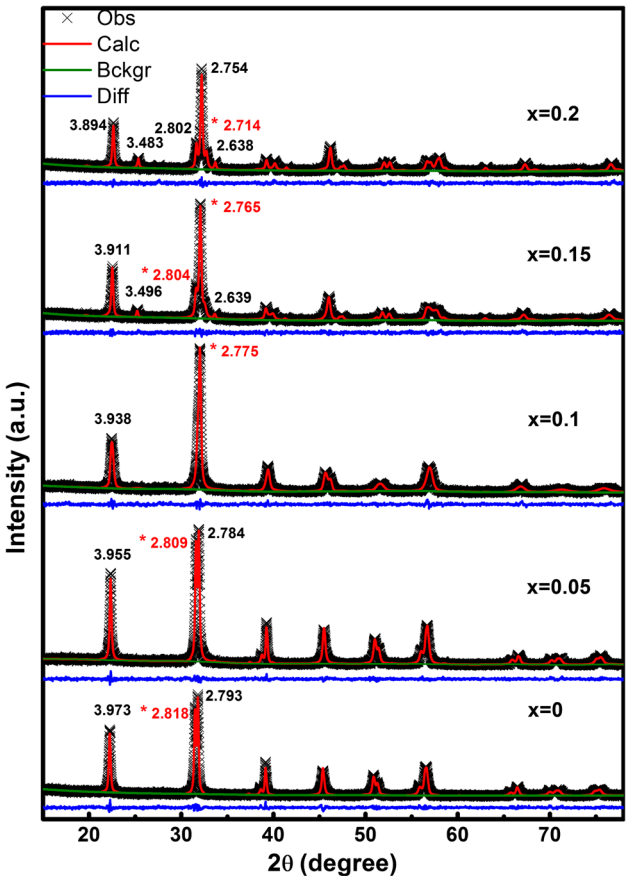

Fig. 2 Rietveld refinements of the pure and Tb-doped $BiFeO_3$ nanoparticles

Table 1 The structural parameters of R3c phase fraction for the pure and Tb-doped $BiFeO_3$ nanoparticles obtained by the Rietveld refinements

$Bi_{1-x}Tb_xFeO_3$	x = 0	x = 0.05	x = 0.1	x = 0.15	x = 0.2
Phase	R3c	R3c + pbnm	R3c + pbnm	R3c + pbnm	R3c + pbnm
R3c phase fraction	1.0000	0.7849	0.6695	0.4590	0.0296
a (Å)	5.6220	5.6192	5.6036	5.5773	5.4944
b (Å)	5.6220	5.6192	5.6036	5.5773	5.6782
c (Å)	13.9713	13.9595	13.8627	13.7277	7.8855
c/a	2.4851	2.4843	2.4739	2.4614	1.4352
V ($Å^3$)	382.422	381.725	376.975	369.812	246.016
R_{wp}	0.0624	0.0527	0.0545	0.0532	0.0550
R_p	0.0489	0.0410	0.0424	0.0416	0.0428
χ^2	0.9290	0.8941	0.9895	0.9620	0.9561

to 20 %, the crystal structure almost completely belongs to Pbnm space group especially.

X-ray photoelectron spectroscopy (XPS) is an excellent technique to investigate the chemical composition and the charge state of the elements presented in the compound [22]. The survey spectrum in Fig. 3a confirms the presence of Bi, Fe, and O in the prepared $BiFeO_3$ sample. The oxidation states of Fe in $BiFeO_3$ nanoparticles were also investigated. The representative scans of the Fe_{2p} lines of the pure and Tb-doped $BiFeO_3$ nanoparticles are shown in Fig. 3b. It is shown that all the positions of Fe $2p_{3/2}$ lines are at around 710 eV, which means the coexistence of Fe^{3+} and Fe^{2+} states [17]. Thus, a detailed examination of the oxidation states of Fe ion is carried out through the peak fitting analysis. The positions of Fe 2p are expected to be at 711 eV for Fe^{3+} and 709.5 eV for Fe^{2+} [23]. The fitting analysis results of Fe $2p_{3/2}$ peaks of $Bi_{1-x}Tb_xFeO_3$ (x = 0, 0.05, 0.1, 0.15 and 0.2) are shown in Table 2. It is worth noting that the fraction of Fe^{3+} increases with the doping concentration of Tb concentration, implying a higher content of Fe^{3+} and lower content of Fe^{2+} after doping with Tb. Thus Tb substitution could depress oxygen vacancies. Apart from this, both the Fe^{3+} and Fe^{2+} peaks fitting lines shift to higher bonding energy, which agrees well with the results obtained from Goldschmidt tolerance factor theory that Fe–O bonds are under compression.

To investigate the effect of Tb substitution on the size of particles, TEM images are shown in Fig. 4. It is shown that the average size of particles calculated from the images in Fig. 4 is 147.05 nm (x = 0), 55.71 nm (x = 0.05), 49.88 nm (x = 0.1), 27.45 nm (x = 0.15), 28.48 nm (x = 0.15), 70.32 nm (x = 0.2), respectively. Noticed that the pure $BiFeO_3$ particles are bigger, which are bigger than 100 nm. While the average size of Tb-doped $BiFeO_3$ particles is smaller than 100 nm, and the particle size decreases with the Tb doping concentration increasing from 0.05 to 0.15. The reduction in particle size is attributed to the addition of Tb^{3+} ions in $BiFeO_3$ lattice, which depresses the grain growth. Furthermore, it is clearly observed that the average sizes of particles become more

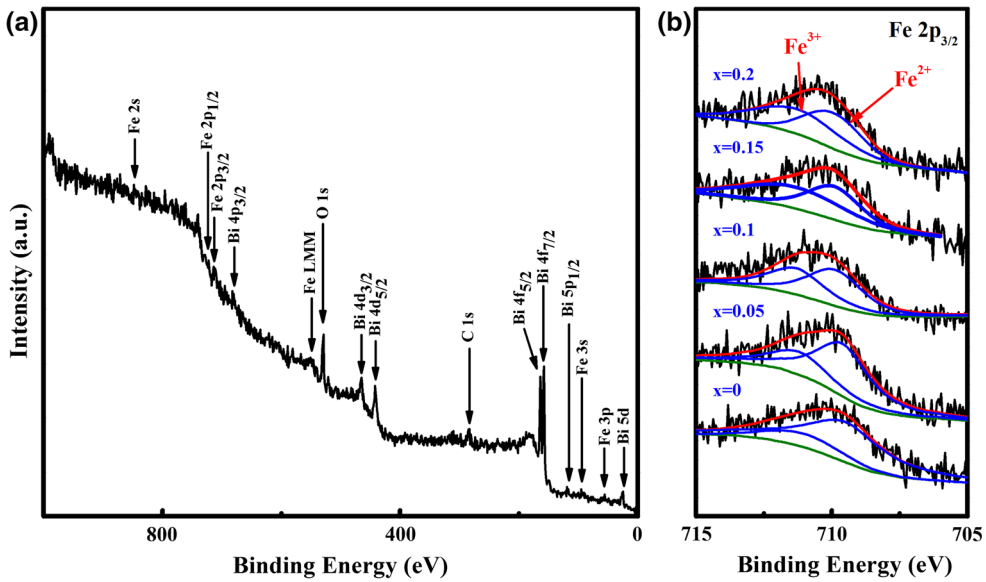

Fig. 3 **a** XPS survey spectra of the pure $BiFeO_3$ nanoparticles. **b** Narrow scan spectra of Fe 2p of $Bi_{1-x}Tb_xFeO_3$ (x = 0, 0.5, 0.1, 0.15 and 0.2) nanoparticles

Table 2 The fitting analysis results of Fe $2p_{3/2}$ peaks of $Bi_{1-x}Tb_xFeO_3$ (x = 0, 0.5, 0.1, 0.15 and 0.2) nanoparticles

Tb concentration x	Fe^{2+} binding energy (eV)	Fe^{3+} binding energy (eV)	Fe^{3+} fraction
x = 0	709.51	711.02	0.1826
x = 0.05	709.6	711.2	0.3364
x = 0.1	709.88	711.31	0.4472
x = 0.15	709.91	711.35	0.5080
x = 0.2	709.94	711.41	0.5259

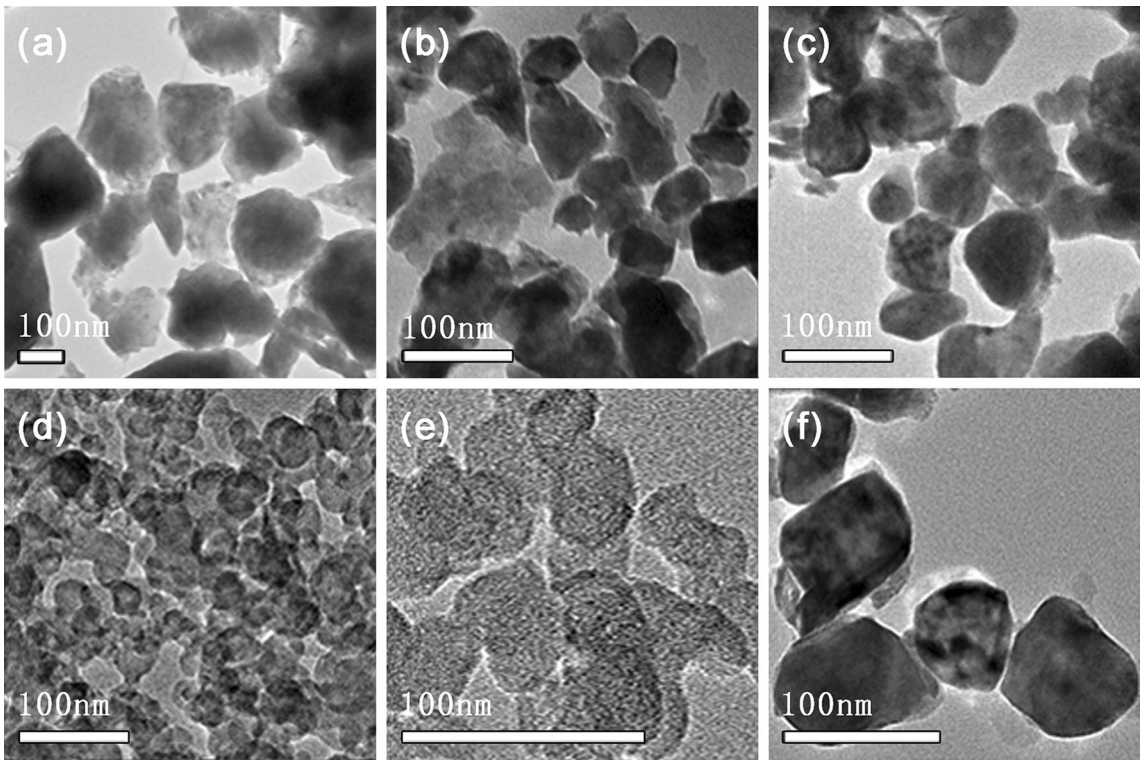

Fig. 4 TEM images of $Bi_{1-x}Tb_xFeO_3$ nanoparticles, **a** x = 0; **b** x = 0.05; **c** x = 0.1; **d** x = 0.15; **e** x = 0.15; **f** x = 0.2

and more smaller with the increasing of Pbnm fraction, when the two phases mentioned above coexist. However, as Tb-doped concentration reaches 0.2, the particle grows large conversely because the crystal structure almost transfers to Pbnm space group. Overall, when only R3c or Pbnm structure exits, particles can grow lager easily.

Figure 5 shows the high resolution TEM images where pronounces lattice fringes, which indicates very good level of crystallinity. Through TEM data analysis software Gatan Digitalmicrograph, the distance between two crystal planes of $Bi_{1-x}Tb_xFeO_3$ is found to be 0.282 nm [(104) in R3c], 0.281 nm [(104) in R3c], 0.278 nm [(112) in Pbnm], 0.280 nm [(020) in Pbnm], 0.277 nm [(112) in Pbnm], 0.271 nm [(200) in Pbnm] for x = 0, 0.05, 0.1, 0.15, 0.15 and 0.2, respectively. Although the interplanar distance above is not from the same crystal planes, the result is in great agreement with interplanar distance calculated from X-ray diffraction showing in Fig. 2. Thus, it is easy to draw a conclusion that the interplanar distance decreases with the increasing of Tb doping concentration compared with the same crystal plane. This result agrees well with the conclusion drawn from XRD Rietveld refinements that unit cell volume (V) decreases with the increasing of Tb doping concentration.

Figure 6 shows magnetic hysteresis loops of the pure and Tb-doped $BiFeO_3$ nanoparticles at room temperature. The pure $BiFeO_3$ demonstrates linear M–H loop with a shift towards negative axis, and its exchange bias field (H_{eb}) equals 100 Oe, as shown in Fig. 6b which indicates that the system exists exchange coupling effect. Bulk $BiFeO_3$ exhibits G-type antiferromagnetic order below Néel temperature [24], so it acts as an antiferromagnetic core. According to the model proposed by Néel for antiferromagnetic nanoparticles based on the presence of two sublattices: one with spins up and another with spins down at the surface. Any imbalance in the number of spins at the

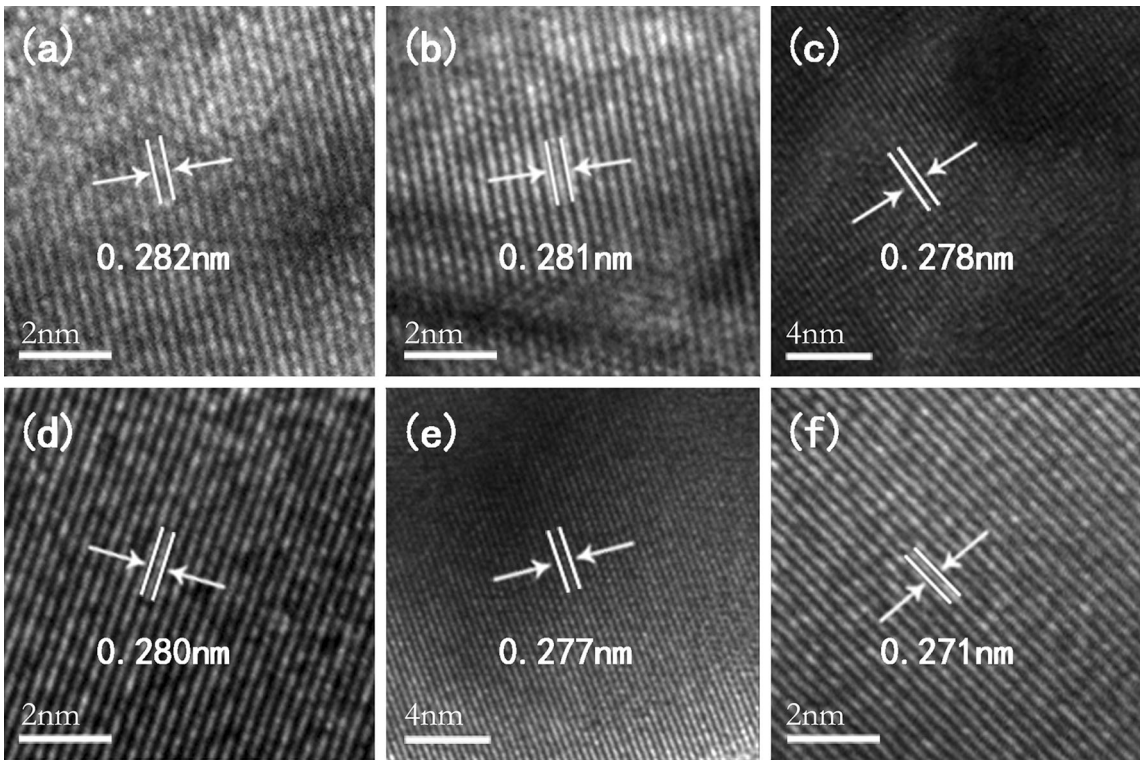

Fig. 5 High resolution TEM images showing the lattice fringes of $Bi_{1-x}Tb_xFeO_3$ nanoparticles, **a** x = 0; **b** x = 0.05; **c** x = 0.1; **d** x = 0.15; **e** x = 0.15; **f** x = 0.2

surface is the origin of a net magnetic moment in "antiferromagnetic" nanoparticles below the ordering temperature of spins [25]. Because the size of grain is smaller than that of bulk $BiFeO_3$, long-range antiferromagnetic order frequently interrupted by grain surface, so uncompensated spins formed at the surface. Compared with bulk $BiFeO_3$, the decrease of grain size in this work makes the surface-to-volume ratio increase, therefore, the role of the surface in the magnetism behaves more important. Indicating that the system exists exchange coupling effect between antiferromagnetic core and ferromagnetic surface. As 5 % Tb was doped, remanent magnetization (M_r), spontaneous magnetization (M_s) and coercivity (H_c) are increased to 0.0469 emu/g, 0.0236 emu/g and 2208.5Oe, respectively, however, H_{eb} decreases to 39.5 Oe, as shown in Fig. 6c. The average size of particles is reduced to 55.71 nm leading to uncompensated spins increased at the surface and strengthened the magnetism in this system. At the same time, Tb^{3+} substituting for Bi^{3+} gives rise to uncompensated spins around Tb^{3+} in antiferromagnetic core which can also strengthen the magnetism [26]. Therefore, the destruction of the long-range antiferromagnetic orders would result in the thinner antiferromagnetic layer, which abates the antiferromagnetic pinning effect. So M_r and H_c increase and H_{eb} decreases. When Tb doping concentration reaches 10 %, M_r, M_s, H_c and H_{eb} are increased to 0.0817, 0.0314 emu/g, 2555.5 and 50.5 Oe, separately, as shown in Fig. 6d. Both the reduction of the average particle size (49.88 nm) and increase of Tb^{3+} substitution result in the improvement of magnetism. So exchange bias field increased either. When Tb-doped concentration x reaches to 0.15, M_r and M_s decrease, while H_c increased slightly. With the average particle size reducing to 27.45 nm, uncompensated spins increase at the surface, which causes the enhanced magnetism. But it is invalid to create additional uncompensated spins by increasing the doping concentration further. Because ions with uncompensated spins in antiferromagnetic layer will be replaced conversely [26], which decreased the magnetism causing magnetic layer became thinning and exchange bias field increased to 129 Oe accompanied with coercive field increased slightly. With Tb-doping concentration increasing to 20 %, M_r and H_c decreases, and almost no spontaneous magnetization phenomenon existed, as shown in Fig. 6f. In addition, uncompensated spins decreased on account of the increase of average particle size and too much dopant. Overall, ferromagnetism and antiferromagnetism became weaken, and the samples presented paramagnetic [27].

Anyway, it is legitimate to infer that the change of magnetism for $Bi_{1-x}Tb_xFeO_3$ (x = 0.05, 0.1, 0.15, 0.2) nanoparticles is attributed to following factors. First of all,

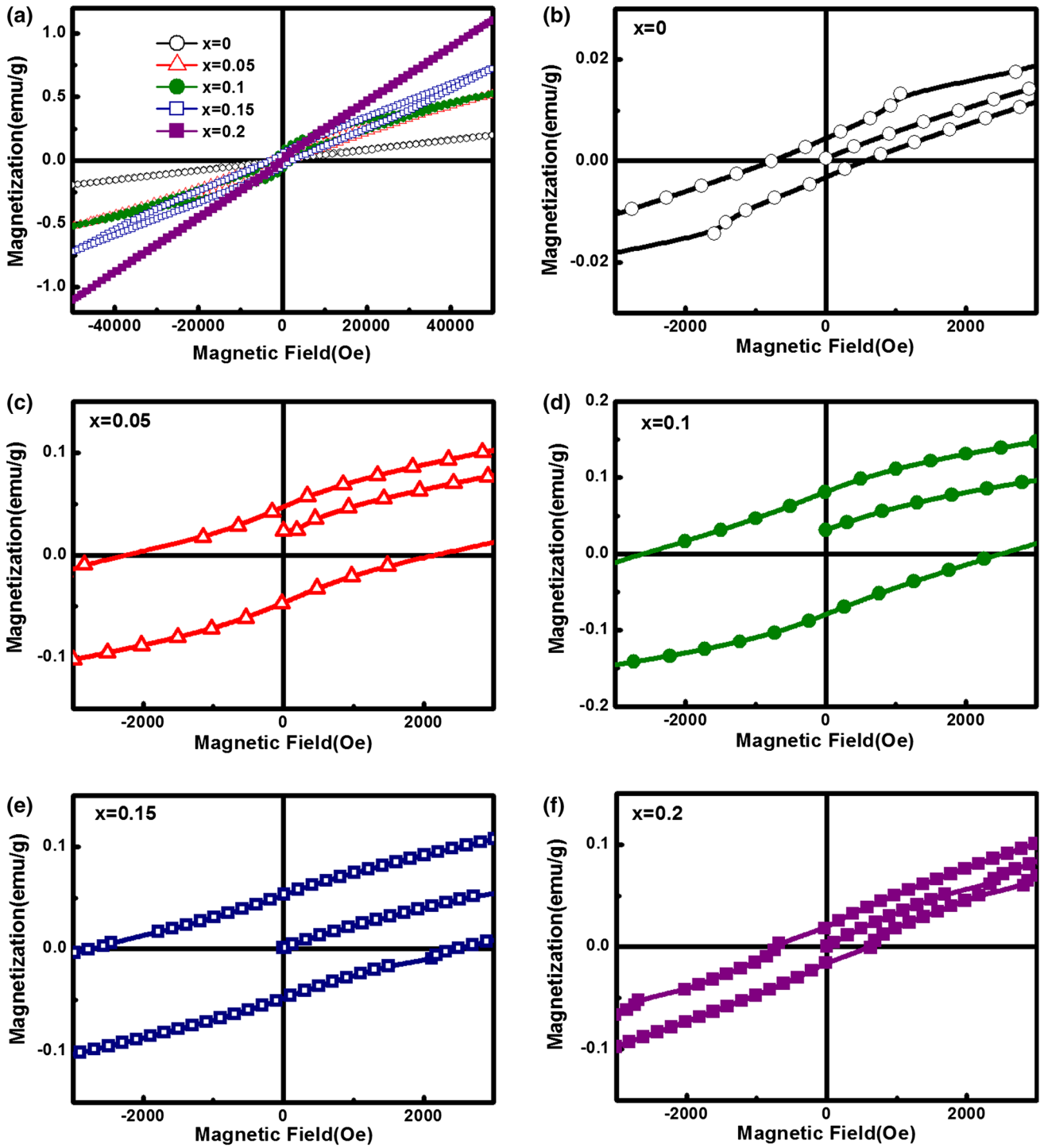

Fig. 6 **a** The magnetization (M)-magnetic field (H) hysteresis loops of the pure and Tb-doped $BiFeO_3$ nanoparticles in room temperature, **b**– **f** zoomed-in view of magnetization hysteresis loops showing the presence of exchange bias coupling of $Bi_{1-x}Tb_xFeO_3$ (x = 0, 0.05, 0.1, 0.15 and 0.2) nanoparticles

a small amount of doping ions make uncompensated spins generate around it and distort its cyclical spin spiral structure belongs to R3c space group. Therefore, the net magnetic moments locked within spiral spin structure are released so that the values of the M_r, M_r and H_c increase gradually with the increase of the Tb-doped concentration x from 0.05 to 0.1. While doping ions increase from 15 % to 20 %, the uncompensated spins in antiferromagnetic layer are replaced by excess doped ions and results in the weaken magnetism, meanwhile, Pbnm phase becomes

dominated which is certified by Rietveld refinements. Secondly, the reduction of particles size causes uncompensated spins augmenting at the surface and to some extent enhancing the magnetism of the samples. Besides, the reduction of Fe^{2+} with the doping concentration increasing leads to the decreasing of magnetism to some degree.

4 Conclusions

The pure and Tb-doped $BiFeO_3$ nanoparticles were prepared using sol–gel method. Tb substitution can reduce the oxygen vacancy and enhance the magnetism. The enhancement of magnetism is attributed to the distortion of the crystal structure and reduction of particle size. Tb substitution suppresses the spiral spin structure and releases the net magnetic moment. At the same time, the reduction of the particle size makes the uncompensated spins at the surface play more important role. The influence of ferromagnetism at the surface becomes more remarkable and the samples demonstrate weak coupling behavior. The present work provides a route to regulate the magnetism of $BiFeO_3$ materials.

Acknowledgments This work was financially supported by the National Natural Science Foundation of China (Grant Nos. 11264026, 11564028), and Inner Mongolia Science Foundation for Distinguished Young Scholars (Grant No. 2014JQ01).

References

1. F.Z. Huang, Z.J. Wang, X.M. Lu, J.T. Zhang, K.L. Min, W.W. Lin, R.X. Ti, T.T. Xu, J. He, C. Yue, J.S. Zhu, Peculiar magnetism of $BiFeO_3$ nanoparticles with size approaching the period of the spiral spin structure. Sci. Rep. **3**, 2907 (2013)
2. C.D. Pham, J. Chang, M.A. Zurbuchen, J.P. Chang, Synthesis and characterization of $BiFeO_3$ thin films for multiferroic applications by radical enhanced atomic layer deposition. Chem. Mater. **27**, 7282 (2015)
3. M. Arora, P.C. Sati, S. Chauhan, H. Singh, K.L. Yadav, S. Chhoker, M. Kumar, Structural, magnetic and optical properties of $B_{i-x}Dy_xFeO_3$ nanoparticles synthesized by sol–gel method. Mater. Lett. **96**, 71 (2013)
4. B. Hu, J.F. Wang, J. Zhang, Z.B. Gu, S.T. Zhang, Synthesis, structures and properties of single phase $BiFeO_3$ and $Bi_2Fe_4O_9$ powders by hydrothermal method. J. Mater. Sci. Mater. Electron. **26**, 6887–6891 (2015)
5. L. Feng, S.W. Yang, Y. Lin, D.L. Zhang, W.C. Huang, W.B. Zhao, Y.W. Yin, S.N. Dong, X.G. Li, Effects of Interface layers and domain walls on the ferroelectric-resistive switching behavior of Au/$BiFeO_3$/$La_{0.6}Sr_{0.4}MnO_3$ heterostructures. ACS Appl. Mater. Interfaces **7**, 26036 (2015)
6. G. Tian, F.Y. Zhang, J.X. Yao, H. Fan, P.L. Li, Z.W. Li, X. Song, X.Y. Zhang, M.H. Qin, M. Zeng, Z. Zhang, J.J. Yao, X.S. Gao, J.M. Liu, Magnetoelectric coupling in well-ordered epitaxial $BiFeO_3$/$CoFe_2O_4$/$SrRuO_3$ heterostructured nanodot array. ACS Nano **2016**, 10 (1025)
7. M. Arora, S. Chauhan, P.C. Sati, M. Kumar, S. Chhoker, Evidence of spin-two phonon coupling and improved multiferroic behavior of $Bi_{1-x}Dy_xFeO_3$ nanoparticles. Ceram. Int. **40**, 13347 (2014)
8. Y.J. Wu, J.G. Wan, C.F. Huang, Y.Y. Weng, S.F. Zhao, J.M. Liu, G.H. Wang, Strong magnetoelectric coupling in multiferroic $BiFeO_3$–$Pb(Zr_{0.52}Ti_{0.48})O_3$ composite films derived from electrophoretic deposition. J Appl. Phys. Lett. **93**, 192915 (2008)
9. J.L. Mi, T.N. Jensen, M. Christensen, C. Tyrsted, J.E. Jørgensen, B.B. Iversen, High-temperature and high-pressure aqueous solution formation, growth, crystal structure, and magnetic properties of $BiFeO_3$ nanocrystals. Chem. Mater. **23**, 1158 (2011)
10. X.G. Huang, J. Zhang, W.F. Rao, T.Y. Sang, B. Song, C.P. Wong, Tunable electromagnetic properties and enhanced microwave absorption ability of flaky graphite/cobalt zinc ferrite composites. J. Alloys Compd. **662**, 409 (2016)
11. X.G. Huang, J. Zhang, Z.H. Liu, T.Y. Sang, B. Song, H.L. Zhu, C.P. Wong, Facile preparation and microwave absorption properties of porous hollow $BaFe_{12}O_{19}$/$CoFe_2O_4$ composite microrods. J. Alloys Compd. **2015**, 648 (1072)
12. Y. Deng, D. Wu, Q. Chen, Y.W. Du, Synthesis, microstructure, magnetic properties and Raman scattering of single-crystalline $BiFeO_3$ nanorods prepared by hydrothermal technique. Optoelectron. Adv. Mater. **6**, 370 (2012)
13. A. Jaiswal, R. Das, K. Vivekanand, P.M. Abraham, S. Adyanthaya, P. Poddar, Effect of reduced particle size on the magnetic properties of chemically synthesized $BiFeO_3$ nanocrystals. J. Phys. Chem. C **114**, 2108 (2010)
14. T.J. Park, G.C. Papaefthymiou, A.J. Viescas, A.R. Moodenbaugh, S.S. Wong, Size-dependent magnetic properties of single-crystalline multiferroic $BiFeO_3$ nanoparticles. Nano Lett. **7**, 766 (2007)
15. V.A. Reddy, N.P. Pathak, R. Nath, Particle size dependent magnetic properties and phase transitions in multiferroic $BiFeO_3$ nano-particles. J. Alloys Compd. **543**, 206 (2012)
16. D.P. Dutta, B.P. Mandal, R. Naik, G. Lawes, A.K. Tyagi, Magnetic, ferroelectric, and magnetocapacitive properties of sonochemically synthesized Sc-doped $BiFeO_3$ nanoparticles. J. Phys. Chem. C **117**, 2382 (2013)
17. Y. Wang, C.W. Nan, Effect of Tb doping on electric and magnetic behavior of BiFeO3 thin films. J. Appl. Phys. **103**, 4103 (2008)
18. J. Liu, H.M. Deng, H.Y. Cao, X.Z. Zhai, J.H. Tao, L. Sun, P.X. Yang, J.H. Chu, Influence of rare-earth elements doping on structure and optical properties of $BiFeO_3$ thin films fabricated by pulsed laser deposition. Appl. Surf. Sci. **307**, 543 (2014)
19. W.Y. Xing, Y.N.N. Ma, Y.L. Bai, S.F. Zhao, Enhanced ferromagnetism of Er-doped $BiFeO_3$ thin films derived from rhombohedral-to-orthorhombic phase transformations. Mater. Lett. **161**, 216 (2015)
20. J. Zhang, Y.J. Wu, X.K. Chen, X.J. Chen, Structural evolution and magnetization enhancement of $Bi_{1-x}Tb_xFeO_3$. J. Phys. Chem. Solids **74**, 849 (2013)
21. P. Ravindran, R. Vidya, A. Kjekshus, H. Fjellvåg, O. Eriksson, Theoretical investigation of magnetoelectric behavior in $BiFeO_3$. Phys. Rev. B **74**, 224412 (2006)
22. M. Gowrishankar, D.R. Babu, S. Madeswaran, Effect of Gd–Ti co-substitution on structural, magnetic and electrical properties of multiferroic $BiFeO_3$. J. Magn. Magn. Mater. **3**, 085 (2016)
23. A. Tamilselvan, S. Balakumar, M. Sakar, C. Nayek, P. Murugavel, K.S. Kumar, Role of oxygen vacancy and Fe–O–Fe bond angle in compositional, magnetic, and dielectric relaxation on Eu-substituted $BiFeO_3$ nanoparticles. Dalton Trans. **43**, 5731 (2014)
24. T.J. Park, G.C. Papaefthymiou, A.J. Viescas, Y. Lee, H.J. Zhou, S.S. Wong, Composition-dependent magnetic properties of

$BiFeO_3$–$BaTiO_3$ solid solution nanostructures. Phys. Rev. B **82**, 024431 (2010)
25. G. Dhir, P. Uniyal, N.K. Verma, Effect of particle size on magnetic and dielectric properties of nanoscale Dy-doped $BiFeO_3$. J. Supercond. Nov. Magn. **27**, 1569 (2014)
26. J.I. Hong, T. Leo, D.J. Smith, A.E. Berkowitz, Enhancing exchange bias with diluted antiferromagnets. Phys. Rev. Lett. **96**, 117204 (2006)
27. J.S. Park, Y.J. Yoo, J.S. Hwang, J.H. Kang, B.W. Lee, Y.P. Lee, Enhanced ferromagnetic properties in Ho and Ni co-doped $BiFeO_3$ ceramics. J. Appl. Phys. **115**, 013904 (2014)